Journal of Sound and Vibration (2002) **255**(1), 147–160
doi:10.1006/jsvi.2001.4145, available online at http://www.idealibrary.com on IDEAL®

HIGH-WAVENUMBER ACOUSTIC RADIATION FROM A THIN-WALLED SCARFED CYLINDER

G. M. KEITH AND N. PEAKE

Department of Applied Mathematics and Theoretical Physics, University of Cambridge, Silver Street, Cambridge CB3 9EU, England

(*Received* 30 *January* 2001, *and in final form* 31 *October* 2001)

The analysis of the radiation from an axisymmetric duct using the Geometrical Theory of Diffraction and uniform asymptotics, presented in a companion paper, is extended to an asymmetric, scarfed cylinder. The generic theory from the application to axisymmetric cylinders is briefly recapitulated and the geometrical calculations necessary for the analysis of the scarfed cylinder are presented in detail. The scarfed cylinder is used as a model for a novel technique of noise reduction in modern aeroengines in which the intake is directed a little upward to try and direct noise radiation away from the ground. We do not carry out a full parameter study, but preliminary results from this work suggest the technique has significant potential noise reduction benefits.

1. INTRODUCTION

In aircraft engines, such as those used on commercial airliners, the fan generates considerable noise, which propagates forward in the engine duct and radiates to the far field from the intake. The geometry of the intake plays an important role in determining the directivity of this radiation.

In the past few years, the aeroacoustics community has engaged in much discussion over an innovative noise control technique called intake scarfing. Rather than directly controlling the noise levels generated by the fan, scarfing attempts, by modifying the shape of the engine intake, to redirect the noise away from the ground and certification microphone locations, and into the atmosphere. A scarfed intake may be thought of as an ordinary intake with the opening face directed slightly upward; see Figure 1.

The asymmetry of the scarfed intake dramatically complicates numerical and analytical investigations into both aerodyamic and noise effects, and the noise issue is further complicated by the high frequencies and correspondingly small wavelengths typical of fan noise. Static testing, which is in any case expensive, is problematic because the effect under investigation is concerned with the specification of the intake geometry and the customary use of a bell-mouthed intake in static testing seriously compromises the applicability of any results acquired.

Several attempts have been made to calculate numerically the radiation from axisymmetric cylinders, but techniques based on finite difference (see, for example, the paper by Li *et al.* [1]), finite element [2], infinite element and boundary element [4] methods can struggle with the typically high wavenumbers. In general, they are used to tackle two-dimensional, axisymmetric problems. To date, no attempt has been made to tackle asymmetric boundary conditions.

0022-460X/02/$35.00

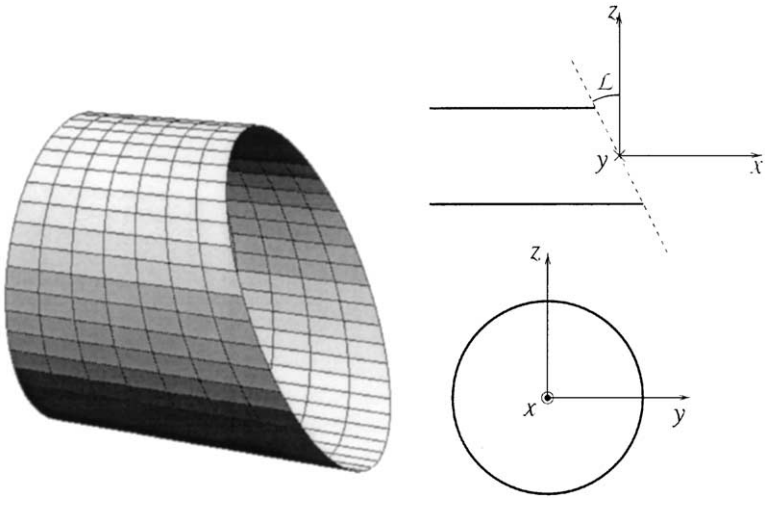

Figure 1. A scarfed cylinder with scarfing angle $\mathscr{L}$.

The Geometrical Theory of Diffraction (GTD) due to Keller [5, 6] describes diffraction effects in high-wavenumber fields. The use of the GTD in the context of acoustic radiation from cylinders, first suggested by Chapman [7], provides an accurate and extremely fast predictive tool and, in addition, a useful paradigm for the interpretation of results.

In this paper, the GTD is applied to the problem of radiation from asymmetric cylinders. The application of the GTD to the axisymmetric cylinder is discussed in detail in the companion paper [8]. That paper contains a detailed discussion of the radiation from a thin-walled axisymmetric cylinder when a single cut-on mode propagates in the duct towards the aperture. The ray description of propagating duct eigenmodes, due to Chapman [7], is used as input to a scattering problem, which is solved by using the GTD. In the first instance a geometrical acoustics field is found, which consists of rays reflected from the inside wall of the duct; next a diffracted field is constructed, which is described by Keller's theory and which consists of rays instigated on the edge by the incident rays. These results had been previously presented by Hocter [9]. However, the GTD breaks down over large regions near singularities at shadow and reflection boundaries and caustics and is inadequate to predict the entire field. The prediction of the phase and amplitude at the peaks of the principal lobe, the region of highest radiated intensity, is particularly poor. To overcome these shortcomings, uniform asymptotic transition fields are employed to smooth the singularities in an asymptotically consistent way.

Due to the nature of the GTD, the only substantial difference between its application to the radiation from axisymmetric and asymmetric cylinders is in the details of the geometry of the various ray fields. Consequently, this paper begins with a very brief recapitulation of the apposite points of the analysis of the radiation from an axisymmetric cylinder. These expressions are then used in the specification of the radiated field in the case of the asymmetric cylinder and they differ from the axisymmetric case only in some of the geometrical quantities that appear in them. The derivation of these geometrical quantities is the subject of section 3, whereafter the machinery is in place to calculate the radiated field. The radiated field is analyzed to draw out some of the effects of scarfing and evaluate and explain its potential efficacy.

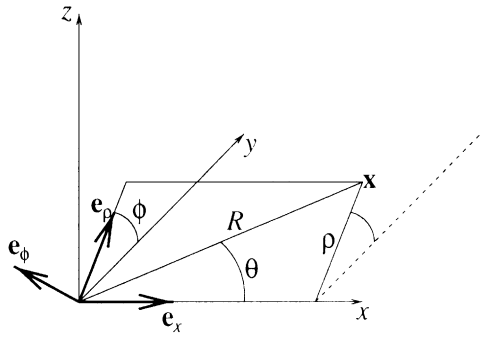

Figure 2. The co-ordinates x. ρ, R, θ, ϕ and the basis vectors $\mathbf{e}_x$, $\mathbf{e}_\rho(\phi)$ and $\mathbf{e}_\phi(\phi)$.

2. THE FIELD RADIATED FROM AN AXISYMMETRIC CYLINDER

The co-ordinate systems shown in Figure 2 are employed, with cylindrical polar co-ordinates x, ρ, ϕ and spherical polar co-ordinates R, θ, ϕ. The unsteady velocity potential u satisfies the Helmholtz equation $\nabla^2 u + k^2 u = 0$, where $k = \omega/c$, ω is the angular frequency of the sound field and c is the speed of sound, which is assumed to be constant. In a semi-infinite duct of radius a, lying along the negative x-axis, propagating eigenmodes may then be written

$$u_{mn} = \mathrm{e}^{\mathrm{i}(m\phi + k_x x)}\, \mathrm{J}_m(k_\rho \rho), \tag{1}$$

where m is the azimuthal mode number and J_m is the Bessel function of order m. The hard wall boundary condition sets $k_\rho a = j'_{mn}$, where n is the radial mode number and j'_{mn} is the nth zero of J'_m. Following Chapman [7], define

$$\sin\theta_{mn} = \frac{j'_{mn}}{ka}, \quad \sin\phi_{mn} = \frac{m}{j'_{mn}}, \quad \rho_{mn} = a\sin\phi_{mn}, \tag{2}$$

where θ_{mn} and ϕ_{mn} are, respectively, the polar and azimuthal mode angles; ρ_{mn} is called the caustic radius and $\rho = \rho_{mn}$ is the caustic cylinder. For $\rho > \rho_{mn}$, the leading-order terms of a high-wavenumber asymptotic expansion of u_{mn} can be described in terms of a family of rays propagating on plane surfaces that are tangential to the caustic cylinder, at the angle θ_{mn} to a line parallel with the cylinder axis in those planes. These rays are described in terms of two further co-ordinates given by

$$0 \leqslant \tilde{\rho} = \sqrt{\rho^2 - \rho_{mn}^2}, \quad \tan\eta = \tilde{\rho}/\rho_{mn}; \tag{3}$$

see Figure 1 in reference [8].

The field on rays reflected from the inside wall of the duct is calculated by the laws of rays theory and ordinary geometrical acoustics. The leading-order term is

$$u_g = A_g(\rho)\, \mathrm{e}^{\mathrm{i}ks_g(x,\rho,\phi) - \mathrm{i}\pi/2} = \mathrm{e}^{\mathrm{i}(n-1)\pi} \left(\frac{1}{2\pi k\tilde{\rho}\sin\theta_{mn}}\right)^{1/2} \mathrm{e}^{\mathrm{i}k(s_i + \sigma_g) - \mathrm{i}\pi/2}, \tag{4}$$

with

$$s_i = \mu_i \rho_{mn}\sin\theta_{mn} + x_i\cos\theta_{mn} \tag{5}$$

and

$$x_i = x - (\tilde{\rho} + \tilde{a})\cot\theta_{mn}, \tag{6}$$

$$\mu_i = \phi - \eta - \eta_{mn}, \tag{7}$$

$$\sigma_g = (\tilde{\rho} + \tilde{a}) \csc \theta_{mn}, \tag{8}$$

where $\tilde{a}$ and η_{mn} are, respectively, the values of $\tilde{\rho}$ and η at $\rho = a$. The geometrical acoustics field is cylindrically divergent and does not satisfy the radiation condition. In the far field, it necessarily falls in the regions requiring the uniform asymptotic transition fields, and these fields return the correct spherical divergence. Nevertheless, the expressions for the geometrical acoustics field are required to construct the uniform transition fields and so must be calculated.

According to Keller's theory, each point on the edge of the cylinder is the vertex to a cone of diffracted rays whose semiangle, β, is equal to the angle between the ray incident on the edge and the tangent to the edge at that point. The leading-order term of the field on the diffracted rays at a given observer location is

$$u_d = A_{\text{inc}} \, e^{ik(s_{\text{inc}} + \sigma)} \frac{D(\tilde{\nu}; \alpha)}{|j|^{1/2}}, \tag{9}$$

where A_{inc} and s_{inc} are, respectively, the amplitude and eikonal of the incident ray at the point of diffraction. The diffraction coefficient, D, is given by

$$D(\tilde{\nu}; \alpha) = \frac{e^{i\pi/4}}{2(2\pi k)^{1/2}} \left[\csc\left(\frac{\tilde{\nu} - \alpha}{2}\right) + \csc\left(\frac{\tilde{\nu} + \alpha}{2}\right) \right] \tag{10}$$

and $\tilde{\nu}$ measures the angle round the cone of diffracted rays from the vector that is perpendicular both to the normal to the surface and to the tangent to the edge at the point of diffraction and that points away from the edge. The angle α is the value of $\tilde{\nu}$ on the continuation of the incident ray past the edge.

The length σ is the distance along the ray to the observer location from the point of diffraction. If $\boldsymbol{\gamma}(\mu)$ describes points on the edge, points insonified by the diffracted rays are in the image of the diffracted ray transformation

$$\mathbf{x} = \boldsymbol{\gamma}(\mu) + \sigma \mathbf{v}(\mu, \nu), \tag{11}$$

where $\mathbf{v}$ is the propagation vector of the diffracted rays on the cones of diffracted rays and ν measures the angle round the cone from the binormal to the edge, which in the case of the axisymmetric cylinder is the unit vector in the x direction. In the axisymmetric case, $\tilde{\nu} = \nu$, but in the asymmetric case $\tilde{\nu} \neq \nu$ and it becomes necessary to distinguish between them. The quantity j in equation (9) is the geometrical divergence of the diffracted ray field and is the determinant of the Jacobian of the diffracted ray transformation, equation (11).

To determine the diffracted field, the ray co-ordinates of a given observer location must be calculated, i.e., the diffracted ray transformation, equation (11), must be inverted. It turns out that, in the far field, there are exactly two or zero solutions to the ray tracing problem, corresponding to there being either two or zero rays through any given point in the far field. A caustic delineates the region into which no rays penetrate from the region in which all points are insonified by two diffracted rays. In this latter region, away from the non-uniform regions discussed below, the field is given by the sum of the contributions from the two diffracted rays and the leading-order terms can be written

$$u_{\text{gtd}} = A_d^+ \, e^{iks_d^+ - i\pi/2} + A_d^- \, e^{iks_d^-}, \tag{12}$$

where $A_d^{\pm}$ and $s_d^{\pm}$ are, respectively, the amplitudes and eikonals of the two diffracted rays that pass through that point. The $\pi/2$ phase retardation on the contribution from the " + "

diffracted ray arises because this ray has passed through the caustic surface. As mentioned above, the influence of the geometrical acoustics field on the far field is only manifested through its role in the construction of the transition fields.

Uniform asymptotics are required near the caustic, where $j = 0$, and near shadow and reflection boundaries, where $\tilde{v} = \pm \alpha$. The caustic transition field is the leading-order term of a uniform asymptotic expansion valid in the caustic transition region near the caustic. It is given on the insonified side of the caustic by

$$u_d = e^{ik\chi} [\mathrm{Ai}(-k^{2/3}\psi) g_0 - ik^{-1/3} \mathrm{Ai}'(-k^{2/3}\psi) h_0], \tag{13}$$

where the prime denotes differentiation with respect to the argument, with

$$\psi = [\tfrac{3}{4}(s_d^+ - s_d^-)]^{2/3}, \quad \chi = \frac{s_d^+ - s_d^-}{2} \tag{14}$$

and

$$g_0 = \sqrt{\pi} k^{1/6} e^{-i\pi/4} (A_d^+ + A_d^-) \psi^{1/4}, \tag{15}$$

$$h_0 = \sqrt{\pi} k^{1/6} e^{-i\pi/4} (A_d^+ - A_d^-) \psi^{-1/4}. \tag{16}$$

The GTD predicts zero amplitude inside the caustic surface in the region into which no rays penetrate. The above expressions may be analytically continued inside the caustic to give a field that decays exponentially to zero.

The shadow and reflection transition fields are the leading terms of a uniform asymptotic expansion valid in the shadow and reflection transition regions near the singularities in the diffraction coefficient. They are given by

$$u = u^+ + u^- \tag{17}$$

with

$$u^+ = e^{iks_g - i\pi/2} A_g \mathscr{F}(k^{1/2} \xi_r) + e^{iks_d^+ - i\pi/2} \left[A_d^+ - \frac{e^{i\pi/4} A_g}{2\sqrt{\pi} k^{1/2} \xi_r} \right], \tag{18}$$

$$u^- = e^{iks_g - i\pi/2} A_g \mathscr{F}(k^{1/2} \xi_s) + e^{iks_d^-} \left[A_d^- - \frac{e^{i\pi/4} A_g}{2\sqrt{\pi} k^{1/2} \xi_s} \right]. \tag{19}$$

Here,

$$\mathscr{F}(z) = -\frac{e^{i\pi/4}}{\sqrt{\pi}} \int_0^z e^{iu^2} du \xrightarrow{z \to \pm \infty} \mp \frac{1}{2} + \frac{e^{i\pi/4} e^{iz^2}}{2\sqrt{\pi} z} \tag{20}$$

and

$$k\xi_r^2 = k(s_d^+ - s_g), \tag{21}$$

$$k\xi_s^2 = ks_d^- - \left[ks_g - \frac{\pi}{2} - 2(n-1)\pi \right], \tag{22}$$

with $k^{1/2}\xi_r$ negative for $-\pi/2 < v^+ < -\alpha$ and positive elsewhere and $k^{1/2}\xi_s$ negative for $-\pi/2 < v^- < \alpha$ and positive elsewhere. The parameters ξ_r and ξ_s are zero on, respectively, the reflection and shadow boundaries. Where both $k\xi_r^2$ and $k\xi_s^2$ are large, the transition expansions return the total field given by the GTD. See reference [10] for a detailed discussion of the derivation of these quantities and their validity in the far field.

3. THE SCARFED CYLINDER

A scarfed cylinder is shown in Figure 1 and the edge is given by

$$\boldsymbol{\gamma}(\mu) = -a\Lambda \sin\mu\, \mathbf{e}_x + \mathbf{e}_\rho(\mu), \tag{23}$$

with $\Lambda = \tan \mathscr{L}$, where $\mathscr{L}$ is the scarfing angle in Figure 1. The tangent to $\boldsymbol{\gamma}$ is $\mathbf{t} = \mathrm{d}\boldsymbol{\gamma}/\mathrm{d}\lambda$ and the normal, $\mathbf{n}$, is given by $\mathrm{d}\mathbf{t}/\mathrm{d}\lambda = \kappa\mathbf{n}$, with $\kappa > 0$, where λ is arc-length around the edge. The binormal is $\mathbf{b} = \mathbf{t} \times \mathbf{n}$ and relationships between the rate of change of $\mathbf{b}$ and $\mathbf{n}$ are given by the Serret–Frenet formulae

$$\frac{\mathrm{d}\mathbf{b}}{\mathrm{d}\lambda} = \tau\mathbf{n}, \qquad \frac{\mathrm{d}\mathbf{n}}{\mathrm{d}\lambda} = -\tau\mathbf{b} - \kappa\mathbf{t}. \tag{24}$$

Referring to the diffracted ray transformation, equation (11), write

$$\mathbf{v}(\mu, \nu) = [\cos\beta(\mu)]\,\mathbf{t}(\mu) + \sin\beta(\mu)\,[(-\sin\nu)\,\mathbf{n}(\mu) + (\cos\nu)\,\mathbf{b}(\mu)]. \tag{25}$$

If $\Pi(\mu)$ is the plane whose normal is $\mathbf{t}$, then $\mathbf{b}$ and $\mathbf{n}$ are contained in Π and ν is the angle the projection of $\mathbf{v}$ on Π makes with $\mathbf{b}$, measured away from $\mathbf{n}$; see Figure 3. The cone angle, β, is the angle between $\mathbf{t}$ and $\mathbf{v}$ and, by Keller's law of diffraction, is equal to the angle between $\mathbf{u}$, the incident ray direction vector, and $\mathbf{t}$, so

$$\mathbf{u} \cdot \mathbf{t} = \mathbf{v} \cdot \mathbf{t}. \tag{26}$$

Furthermore, by using the Serret–Frenet formulae, it may be shown that

$$j = \frac{\partial(x, y, z)}{\partial(\lambda, \nu, \sigma)} = \frac{\partial\mathbf{x}}{\partial\sigma} \cdot \left(\frac{\partial\mathbf{x}}{\partial\lambda} \times \frac{\partial\mathbf{x}}{\partial\nu}\right) = \sigma\,(\sin^2\beta)\,(1 + K\sigma), \tag{27}$$

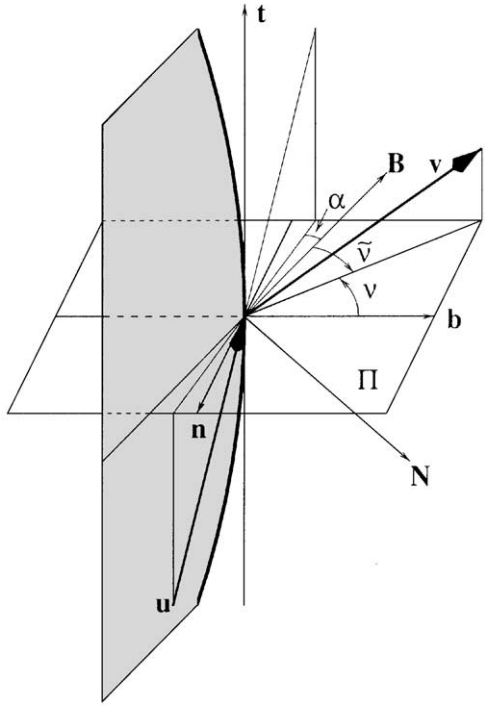

Figure 3. A diffracted ray from a general curved edge with its incident ray.

with

$$K = \frac{\kappa \sin v - \mathrm{d}\beta/\mathrm{d}\lambda}{\sin \beta} \tag{28}$$

and $\mathrm{d}\beta/\mathrm{d}\lambda$ is found by differentiating equation (26).

To find $\tilde{v}$ and α, the vector that is perpendicular to both the normal of the cylinder surface and the tangent to the edge at the point of diffraction is required. If $\mathbf{N}(\mu)$ is the normal to the surface at the point of diffraction, the surface binormal is defined by $\mathbf{B} = \mathbf{t} \times \mathbf{N}$ and $\mathbf{N}$ is chosen so that $\mathbf{B}$ points away from the surface. The angle $\tilde{v}$ is the angle between the projection of $\mathbf{v}$ on Π and $\mathbf{B}$, measured away from $\mathbf{N}$. In the axisymmetric case, $\mathbf{b} = \mathbf{B}$ and $\mathbf{n} = \mathbf{N}$, but this is not the case with scarfing. The amplitude and eikonal on rays incident on the edge, required to calculate the diffracted ray amplitude and eikonals, are given by

$$A_{\mathrm{inc}} = A_g(a), \quad s_{\mathrm{inc}} = s_g(\boldsymbol{\gamma} \cdot \mathbf{e}_x, a, \mu). \tag{29}$$

All that remains to determine the diffracted field is to calculate the ray co-ordinates of a given observer location, i.e., to invert the diffracted ray transformation, equation (11). Taking the inner product of equation (11) with $\mathbf{t}$ and noting that, for a given $\mathbf{x}$, $\sigma = |\mathbf{x} - \boldsymbol{\gamma}|$, gives an implicit algebraic equation for μ

$$[\mathbf{x} - \boldsymbol{\gamma}(\mu)] \cdot \mathbf{t}(\mu) = |\mathbf{x} - \boldsymbol{\gamma}(\mu)| \mathbf{u}(\mu) \cdot \mathbf{t}(\mu), \tag{30}$$

which is solved numerically. Based on experience with the diffracted ray field of axisymmetric cylinder radiation, it is reasonable to expect to find two regions delineated by a caustic; in one of which points are insonified by two rays, i.e., there are two solutions of equation (30); and no rays penetrate into the other, i.e., equation (30) has no solutions. This indeed turns out to be the case, and the topology of the ray field with scarfing, at least for modest scarfing angles, is identical to that of the axisymmetric case. Once values for μ have been determined for a given observation point, it is simple to calculate values for σ, v, $\tilde{v}$, α and β.

To calculate the far-field velocity potential, simply employ equations (4)–(22) using the geometrical quantities derived above.

Away from the shadow and reflection boundaries and caustic, the various transition expansions, when evaluated asymptotically, return the field predicted by the GTD. Where the transition field differs from the field predicted by the GTD by an amount greater, asymptotically, than the first neglected term of the GTD expansion, the transition expansions are employed. Elsewhere, the field is given by equation (12). Encouraged by the excellent agreement between the results obtained using the present theory and the exact analytical results in the axisymmetric case (see Figures 7–9 in reference [8]), there is good reason to suppose that the present theory is comparably accurate in predicting these fields and their interaction in the scarfed case.

However, there is a further class of rays in the scarfed case for which no account has yet been made. These are rays diffracted in the first instance from the edge that are then reflected, possibly several and, in principle, arbitrarily many times, from the duct wall before being radiated into the far field. These rays insonify a region between the two cones $\theta = \pi/2 \pm \mathscr{L}$ and carry a field comparable in magnitude to the diffracted field in that region. Despite confidence in the accuracy of our theory at predicting the primary diffracted rays and the various transition fields, there cannot be similar confidence that the detail of the field in that region is accurately rendered with the present theory.

Integral measures of the radiated field are dominated by contributions from the principal lobe, which is accurately predicted in the axisymmetric case with the present theory and

which would not be substantially modified by this extra class of rays. Therefore, the results pertaining to total radiated intensity ought to be adequate for the purpose of realistically discussing the effects of scarfing on the total upward and downward radiation of sound.

4. RESULTS

The far-field potential takes the form

$$u \sim \Omega(\theta, \phi; ka)\,\frac{e^{ikR}}{kR} \tag{31}$$

and it may be shown that $|kRu|$ is a reasonable approximation to $\Omega = \lim_{R\to\infty} |kRu|$ if

$$R > \mathscr{R}_{\mathscr{L}} = \frac{[2a\cos(\theta_{mn} - \mathscr{L})\cos\phi_{mn}]^2}{\lambda\cos^2\mathscr{L}};$$

see reference [10]. This distance acts in this problem as the Fresnel distance in the problem of diffraction of a plane wave by an aperture, it delineates the near-field Fresnel diffraction zone from the far-field Fraunhofer diffraction zone. These distances are also related to the Rayleigh distance encountered in a class of radiation problems, which once again gives an estimate of the distance where the transition from near- to far-field behaviour takes place.

A full description of the directivity $|kRu|$ in the axisymmetric case is given in the previous paper [8]. Broadly, the quiet region into which no rays penetrate is delineated by a caustic, which, in the axisymmetric case, is approximately located by an angle $\theta = \theta_m$, where $\sin\theta_m = m/ka$. The principal lobe, corresponding to the region of highest radiated intensity, is located around $\theta = \theta_{mn}$. For larger polar angles, forward of the plane of the duct aperture ($x = 0$), there is a region insonified by two diffracted rays. Behind this plane, one of the rays is trapped in the duct and the far field is insonified by a single diffracted ray up to a rearward pointing caustic (Figure 4).

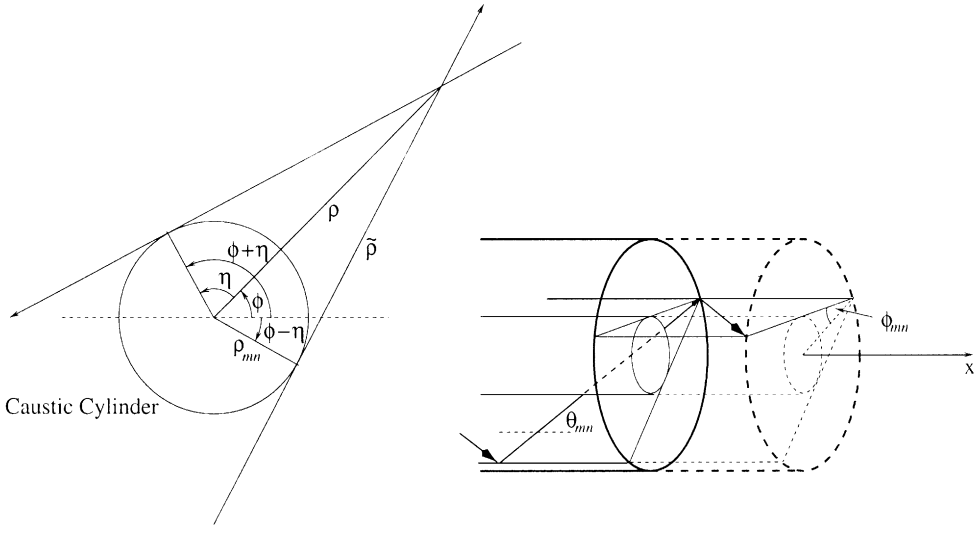

Figure 4. A plan view of two rays and the caustic cylinder, with ρ_{mn}, $\tilde{\rho}$ and η and a Chapman ray propagating along the duct and forming part of a piecewise linear helix.

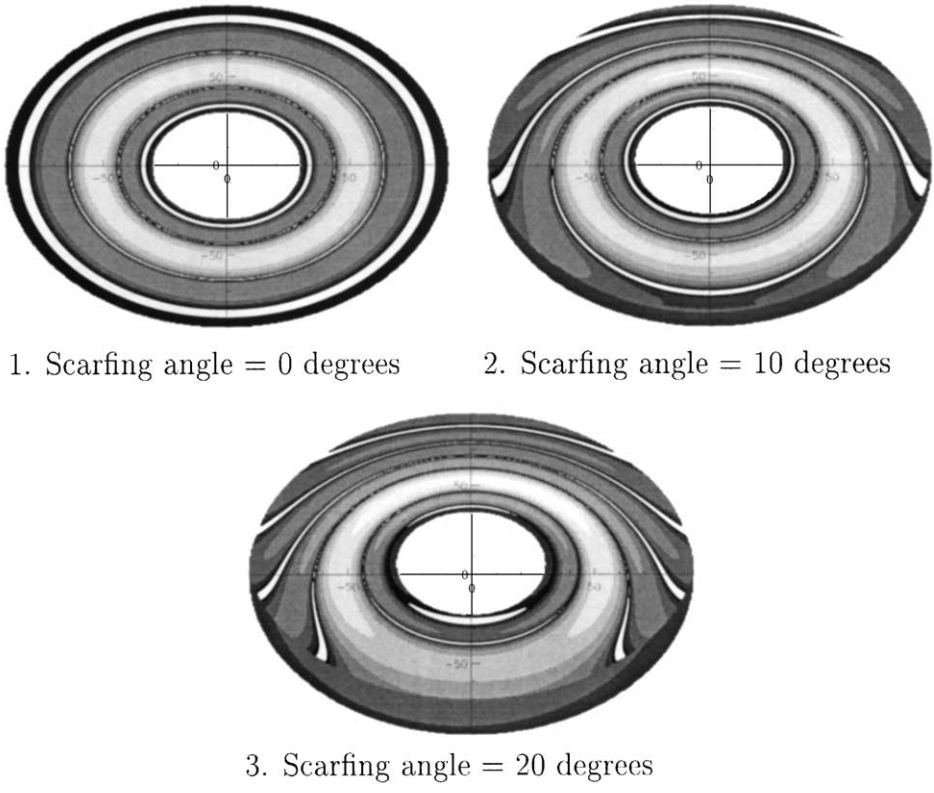

Figure 5. Contour plot of predicted directivity when a single mode, $ka = 40, m = 20, n = 3$, propagates in a duct with various scarfing angles.

Figures 5 and 6 show contour plots of the far-field directivity resulting from the geometrical acoustics and primary diffracted fields when a single mode propagates in the duct towards the aperture, with scarfing angle increasing in 10° increments from 0 to 30°. The final plot is shown together with directivity profiles taken along certain meridional planes. The mode used here has $ka = 40$, $m = 20$ and $n = 3$ and is based on the blade passing frequency and number of blades of a typical aeroengine. The ability to handle such large values of ka is a particular feature of our asymptotic method and is crucial in practice.

In the contour plots, linear distance along a radius on the plot corresponds to polar angle, $0 < \theta < 90^\circ$, and the angle from the horizontal, measured anticlockwise, corresponds to the azimuthal angle ϕ. Effectively, these figures show the projection of the directivity onto the hemisphere forward of the duct aperture. The directivity profiles are for $0 < \theta < 180^\circ$ and, in addition, show the field behind the $\theta = 90^\circ$ plane.

The effect of scarfing in the forward region, broadly, is to move the caustic, and with it the quiet region, upwards towards the principal lobe, which is intensified above the horizontal and attenuated below. Other features that become apparent as the scarfing angle increases are the loss of left–right symmetry and the increased extent of a region of low sound level with no interference fringing below the horizontal. This latter feature arises as more rays are obstructed by the duct wall extending below the horizontal and corresponds to the region, now enlarged, below the horizontal, which is insonified by only one diffracted ray. The absence of left–right symmetry arises from the interaction between the rotational, but not left–right reflectional, symmetry of the incident duct mode and the left–right reflectional,

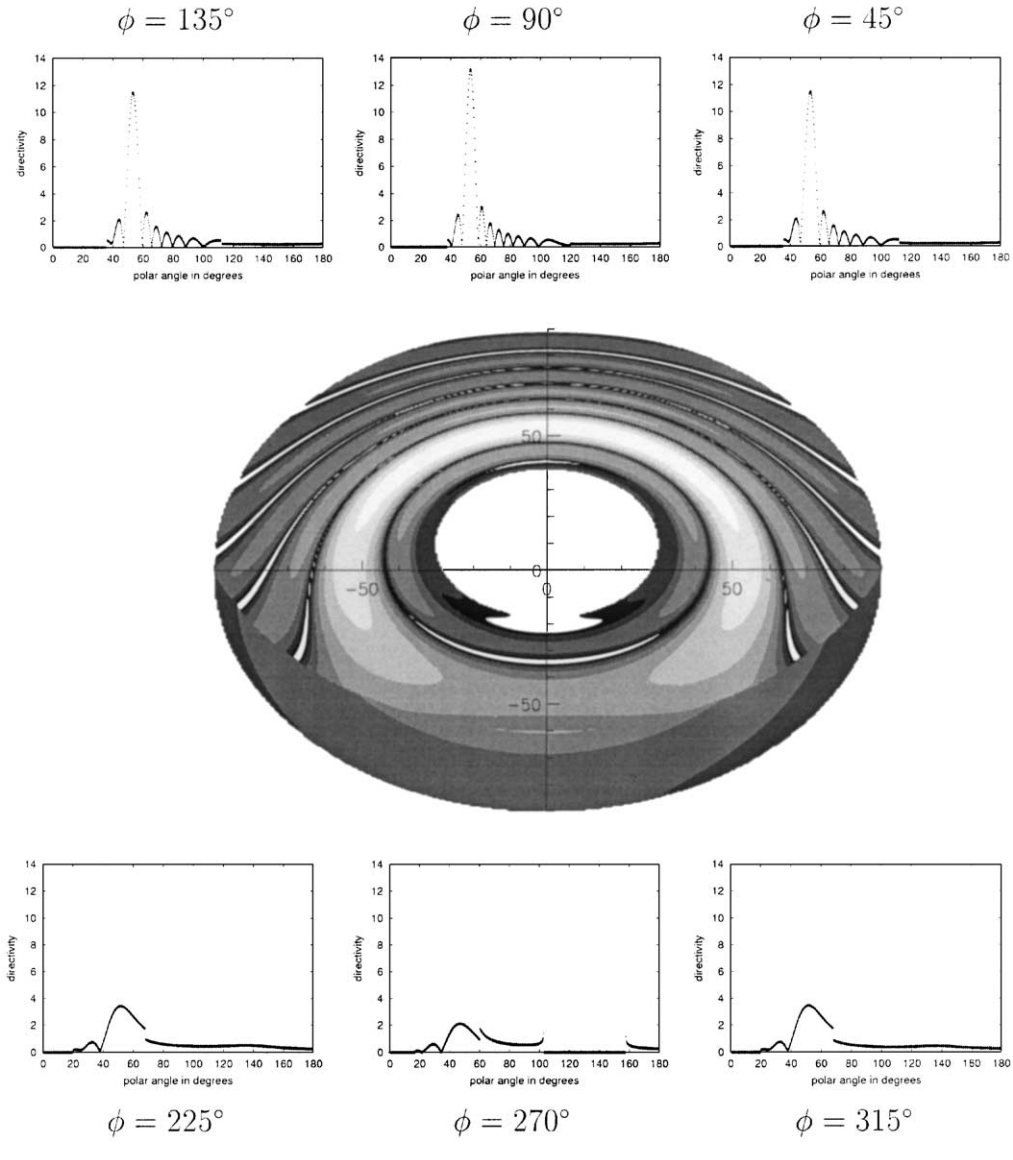

Figure 6. Contour plot of predicted directivity when a single mode, $ka = 40$, $m = 20$, $n = 3$, propagates in a duct with a scarfing angle of 30°; together with directivity profiles (plotted to the same scale) taken along selected meridional planes.

but not rotational, symmetry of the boundary geometry. In the rearward region, the primary effects of scarfing are the movement of the rearward quiet region and the increase in the extent of the region insonified by two diffracted rays above the horizontal and its decrease below. The action of scarfing on the rearward quiet region can be seen in the directivity profile for $\phi = 270°$, where the entire quiet region has slipped below the horizontal. The movement of the point where one of the rays is trapped by the duct can clearly be seen in the directivity profiles of the upward azimuthal directions.

To evaluate the effectiveness of scarfing in redirecting total sound power level, the square of the modulus of the sound field, which is proportional to the radiated intensity, is

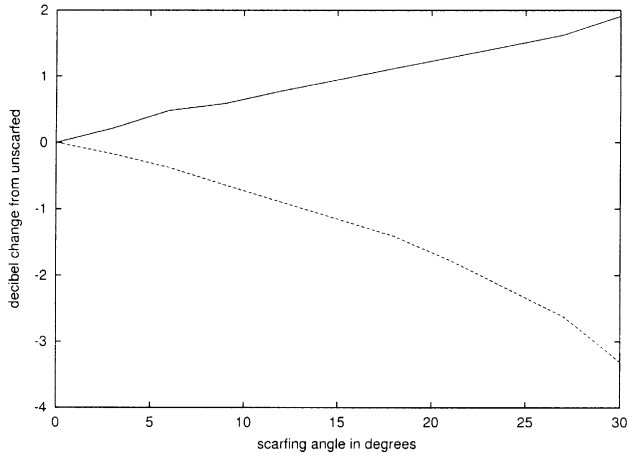

Figure 7. The change in integrated sound power level above and below the horizontal from unscarfed to scarfed ducts with a single mode propagating in the duct.

integrated between $\theta = 0$ and 120° for $0 < \phi < 180^\circ$ and $180^\circ < \phi < 360^\circ$, i.e., above and below the horizontal. The range of θ is chosen to include all the major effects of scarfing on the forward field and back to the plane of the aperture in the case of the greatest scarfing (30°). The decibel change from the unscarfed case is plotted against scarfing angle in Figure 7. The mode used in this calculation is the same as was used in the production of the contour plots.

The total integrated sound power level below the horizontal is decreased, apparently at the expense of a comparable increase in sound power level above the horizontal. The steepening of the lower curve is due to the intrusion into the range of integration of the rearward quiet region.

Figure 8 shows the directivity patterns of modes with a variety of wavenumbers and with different radial orders. The increase in interference fringing can clearly be seen as ka is increased from 20 to 60 in plots 1–3.

With well cut-on modes, such as in plot 4 in Figure 8, the directivity is highest close to the caustic and scarfing is expected to have the least effect on such modes. Conversely, we expect scarfing to have its greatest effect on nearly cut-off modes such as in plot 6 of Figure 8.

Scarfing is expected to be most effective where the polar mode angle, θ_{mn}, is so large that some of the edge is not insonified by rays reflected from the duct. These techniques as they stand are unable to deal with this case, although slightly more sophisticated ray tracing would quickly render these cases accessible so long as the reflection transition region is contained away from the face of the aperture.

Figure 9 shows the change in intensity integrated over $0 < \theta < 120^\circ$ above and below the horizontal when various modes propagate in a duct scarfed by 30°. As expected, scarfing is increasingly efficacious as the mode is increasingly cut off.

5. CONCLUSION

It is shown in the companion paper [8] that the Geometrical Theory of Diffraction, when employed together with the necessary uniform asymptotic theory, provides extremely fast

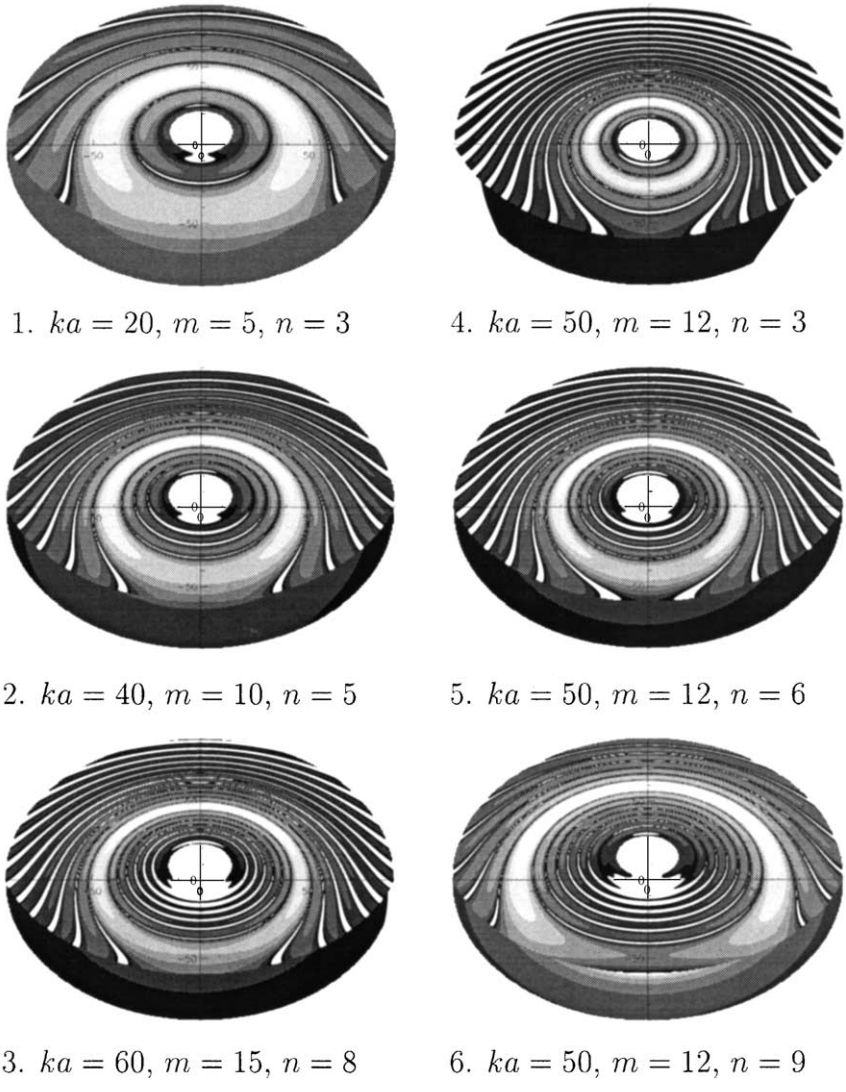

Figure 8. Filled contour plot of predicted directivity when various modes are propagating in a duct with 30° scarfing.

and remarkably accurate predictions of both the amplitude and phase of the far-field directivity of the radiation when propagating eigenmodes are incident on the end of a semi-infinite axisymmetric duct. This paper shows that the great advantage of the GTD is not merely its speed and accuracy, but also its ability to cope with asymmetries in the boundary configuration. The differences in the calculation of the radiated field from axisymmetric and asymmetric cylinders are entirely geometrical; even the problem of the diffracted–reflected rays is essentially one of ray tracing.

Although it is reasonable to suppose that the primary diffracted field and the uniform asymptotic transition fields account for the leading-order behaviour of the far-field directivity and are sufficient to inform a discussion on the effects of scarfing, there are several issues outstanding that require further attention. The first is the ray tracing associated with the diffracted–reflected ray field, which will bring about changes in a small

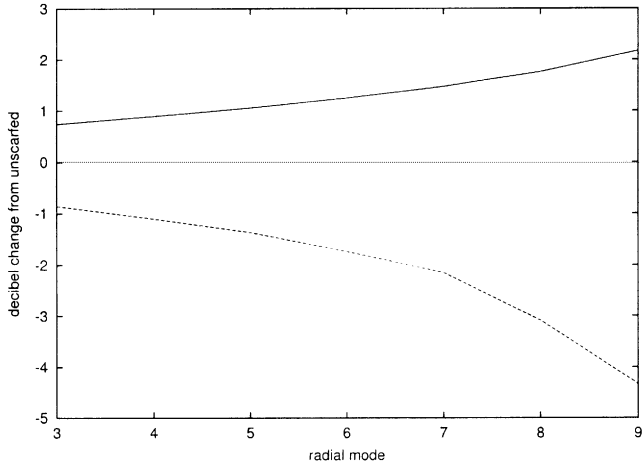

Figure 9. Decibel change in integrated sound power level from unscarfed for various radial modes.

region of the far field, as discussed in section 3. Although a full account of these rays will certainly impact on the exact detail of the far-field directivity in these regions, they will not affect the broad structure of the far field, nor affect the conclusions arrived at on the qualitative effects of scarfing. At present the theory breaks down when the scarfing angle is large enough that the caustic transition region overlaps with the reflection transition region although, as was shown in our previous paper [8], the onset of this difficulty can be substantially reduced either, if appropriate, by looking far out into the far field, or by exploiting the small size of the second terms in the asymptotic expansions of the uniform transition expansions; see reference [10] for a full discussion. This difficulty can be resolved by using a third type of uniform asymptotic expansion, based on the Airy–Fresnel function; see reference [11]. At greater scarfing angles, the reflection transition zone is rescattered from the cylinder edge. Methods of dealing with problems such as these are also presented by Borovikov and Kinber [11]. Finally, for even greater scarfing angles, not all of the lip is insonified by the incident mode, and the problem of the ray tracing of the diffracted–reflected rays must once again be addressed.

All these large scarfing angle difficulties affect the modes which are closest to cutoff. These modes are thought to respond most favourably to scarfing and the results we acquire for the better cut-on modes are the worst case and, therefore, the most pertinent. Conclusions regarding the efficacy of scarfing are certain to be more favourable for the nearly cut-off modes than for the modes that can be treated by the method as it stands.

In order to evaluate the efficacy of scarfing, a number of different modes and wavenumbers should be studied in a large parameter study. The preliminary indications are, however, most encouraging. Scarfing appears to decrease the radiation directed downwards at the expense of an increase in radiation directed upwards.

ACKNOWLEDGMENTS

The authors would like to thank the EPSRC and Rolls-Royce plc for their generous assistance to this research and Dr Hubert Meitz for his valuable advice and ongoing contribution.

REFERENCES

1. X. D. Li, L. P. Xue, J. P. Yan and F. Thiele 1999 *Proceedings of the* 6*th* II*AV International Congress on Sound and Vibration*. Parallel computation of duct acoustics by computational acoustics approach.
2. W. Eversman and I. D. Roy 1999 *Proceedings of the AIAA Aeroacoustics, paper # AIAA*-99-1823. A new reflection free boundary in uniform flow using mapped infinite wave envelope elements.
3. J. R. Astley 1999 *Proceedings of the* 6*th* II*AV International Congress on Sound and Vibration*. Infinite elements for acoustics.
4. P. M. Juhl 1999, *Proceedings of the* 6*th* II*AV International Congress on Sound and Vibration*. Radiation from a lined duct in uniform flow using the boundary element method.
5. J. B. Keller 1958 *Calculus of Variations and its Applications, Proceedings of Symposia on Applied Mathematics* **8**, 27–52. A geometrical theory of diffraction.
6. J. B. Keller 1962 *Journal of the Optical Society of America* **52**, 116–130. Geometrical theory of diffraction.
7. C. J. Chapman 1994 *Journal of Fluid Mechanics* **281**, 293–311. Sound radiation from a cylindrical duct. Part 1. Ray structure of the duct modes and of the external field.
8. G. M. Keith and N. Peake 2002 *Journal of Sound and Vibration* **255**, 129–146. High-wavenumber acoustic radiation from a thin-walled axisymmetric cylinder.
9. S. T. Hocter 2000, *Journal of Sound and Vibration* **231**, 1243–1256. Sound radiated from a cylindrical duct with Keller's geometrical theory.
10. G. M. Keith 2001 *Ph. D. Thesis, University of Cambridge*. A theoretical investigation into the acoustic radiation from an aeroengine intake.
11. V. A. Borovikov and B. Y. Kinber 1994 *Geometrical Theory of Diffraction*. London: Institution of Electrical Engineers.